

Supporting Information for

Low variability of single-molecule conductance assisted by bulky metal-molecule contacts

Rubén R. Ferradás,^{a,b} Santiago Marqués-González,^{c,d} Henry M. Osorio,^{e,f,g} Jaime Ferrer,^{a,b} Pilar Cea,^{e,f} David C. Milan,^h Andrea Vezzoli,^h Simon J. Higgins,^h Richard J. Nichols,^h Paul J. Low,^{*,c} Víctor M. García-Suárez,^{*,a,b} Santiago Martín^{*,e,i}

^a *Nanomaterials and Nanotechnology Research Center, University of Oviedo & CSIC, 33007 Oviedo, Spain.*

^b *Departamento de Física, Universidad de Oviedo, 33007 Oviedo, Spain.*

^c *School of Chemistry and Biochemistry, University of Western Australia, 6009, Australia.*

^d *Department of Chemistry, Graduate School of Science and Engineering, Tokyo Institute of Technology, Tokyo 152-8511, Japan.*

^e *Departamento de Química Física, Facultad de Ciencias, Universidad de Zaragoza, 50009 Zaragoza, Spain.*

^f *Instituto de Nanociencia de Aragón (INA) and Laboratorio de Microscopías Avanzadas (LMA), Edificio i+d. Campus Rio Ebro, Universidad de Zaragoza, C/Mariano Esquillor, s/n, 50017 Zaragoza, Spain.*

^g *Departamento de Física, Escuela Politécnica Nacional, Av. Ladrón de Guevara, E11- 253, 170525 Quito, Ecuador.*

^h *Department of Chemistry, University of Liverpool, Liverpool, L69 7ZD, United Kingdom.*

ⁱ *Instituto de Ciencia de Materiales de Aragón (ICMA), Universidad de Zaragoza-CSIC, 50009 Zaragoza, Spain.*

1. Synthesis of 4 and 6

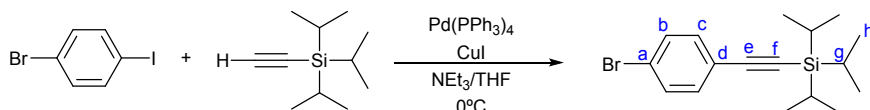
General Conditions

All reactions were carried out in oven dried glassware under an oxygen-free nitrogen atmosphere using standard Schlenk techniques. Reaction solvent NEt_3 was dried over CaSO_4 and distilled under nitrogen. Other reaction solvents were purified and dried using Innovative Technology SPS-400 and degassed before use. The compounds $\text{Pd}(\text{PPh}_3)_4$,¹ $\text{PdCl}_2(\text{PPh}_3)_2$,² 4-bromoiodobenzene,³ 4-bromotolan,⁴ and 1,4-diethynylbenzene⁵ were prepared by the literature methods. Other reagents were purchased commercially and used as received.

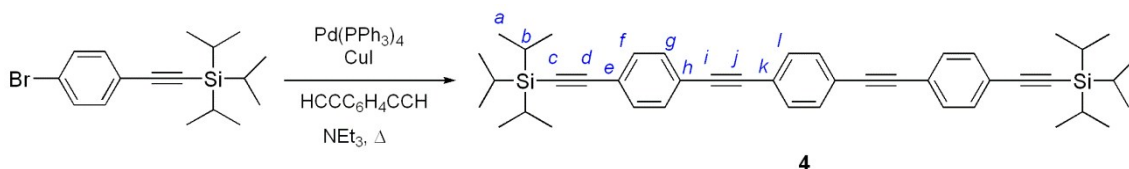
NMR spectra were recorded in deuterated solvent solutions on Varian Mercury-200 and 400, Bruker Avance-400, Varian Inova-500, and Varian VNMRS 600 and 700 spectrometers and referenced against solvent resonances (^1H , ^{13}C)⁶ or external H_3PO_4 (^{31}P) or tetramethylsilane (^{29}Si $\delta = 0.0$ ppm). ASAP mass spectra were recorded from solid aliquots on an LCT Premier XE mass spectrometer (Waters Ltd, UK) or Xevo QToF mass spectrometer (Waters Ltd, UK) in which the aliquot is vaporized using hot N_2 , ionized by a corona discharge and carried to the TOF detector (working range 100-

1000 m/z). Infrared spectra were recorded from Nujol mulls on NaCl plates or dichloromethane solutions in CaF₂ windowed solutions cells, using a Nicolet Thermo FT6700 spectrometer.

Synthesis of 4



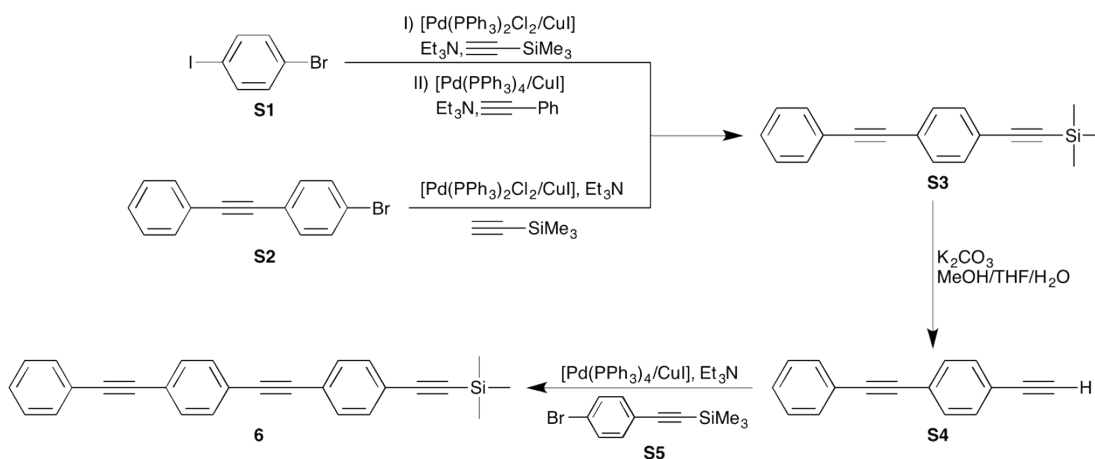
Preparation of BrC₆H₄C≡CSiPr₃.⁷ In a 250 mL Schlenk flask charged 1-bromo-4-iodobenzene (1.01 g, 3.58 mmol), Pd(PPh₃)₄ (0.198 g, 0.171 mmol) and CuI (0.032 g, 0.168 mmol) were suspended into an ice cold mixture of THF (100 mL) and NEt₃ (10 mL). To that mixture ethynyltriisopropylsilane (0.80 mL, 3.6 mmol) was added drop wise during 15 minutes and the mixture stirred at 0 °C for 5 hours. The yellow suspension was allowed to warm to room temperature and stirred overnight. The mixture was filtered and the filtrate purified by chromatography on silica gel using hexane as the eluent. Removal of solvent from the main fraction yielded the pure product as a colourless oil. Yield 1.13 g, 3.35 mmol, 94%. ¹H NMR (400 MHz, CDCl₃) δ 7.24 (d, *J* = 9 Hz, 2H, *c*), 7.14 (d, *J* = 9 Hz, 2H, *b*), 0.93 (s, 21 H, *g/h*). ¹³C {¹H} NMR (101 MHz, CDCl₃) δ 133.6, 131.58 (*b/c*), 122.6 (*a/d*), 106.0, 92.2 (*e/f*), 18.8 (*g*), 11.4 (*h*). IR (*nujol*) cm⁻¹: 2159 (*s*) ν(C≡C).



Preparation of 4.⁸ A 25 mL Schlenk flask charged with HC≡CC₆H₄C≡CH (0.054 g, 0.428 mmol), BrC₆H₄C≡CSiPr₃ⁱ (0.29 g, 0.86 mmol), Pd(PPh₃)₄ (0.05 g, 0.04 mmol) and CuI (0.01 g, 0.05 mmol) and NEt₃ (15 mL) was stirred at reflux overnight. The reaction mixture was filtered and the yellow filtrate taken to dryness. The residue was purified by silica gel column chromatography (hexane). A yellow residue obtained after solvent evaporation from the main fraction. The pure product was obtained as white needles upon crystallization from hexane. Yield 0.16 g, 0.26 mmol, 61%. ¹H NMR (400 MHz, CDCl₃) δ 7.51 (s, 4H, *f*), 7.45 (s, 8H, *g/l*), 1.14 (s, 42H, *a/b*). ¹³C {¹H} NMR (101 MHz, CDCl₃) δ 132.2, 131.7, 131.5 (*f/g/l*), 123.7, 123.2, 123.0

(e/h/k), 106.8, 93.2 (c/d), 91.2, 91.0 (i/j), 18.8 (b), 11.5 (a). MS⁺ (ASAP) *m/z* (%): 638.36 (100, [M]⁺).

Synthesis of 6



Preparation of 4-(Trimethylsilylethynyl)tolan (S3).

Method 1: Ethynyltrimethylsilane (1.77 g, 18.0 mmol) was added to a solution of 1-bromo-4-iodobenzene (5.00 g, 17.7 mmol), PdCl₂(PPh₃)₂ (124 mg, 177 μmol) and copper(I) iodide (34.0 mg, 177 μmol) in triethylamine (125 mL) and the reaction mixture was stirred at room temperature for 16 h. Subsequently, ethynylbenzene (1.82 g, 17.9 mmol), Pd(PPh₃)₄ (817 mg, 707 μmol) and copper(I) iodide (135 mg, 707 μmol) were added and the reaction mixture was heated to reflux for 3.5 h. Following cooling to ambient temperature the solvent was removed under reduced pressure and the residue was purified by flash column chromatography (silica gel; eluent, hexanes) followed by recrystallization from ethanol to afford **S3** in 70% yield (3.36 g, 12.3 mmol) as a white crystalline solid.

Method 2: Ethynyltrimethylsilane (898 mg, 9.15 mmol) was added to a solution of 4-bromotolan (1.96 g, 7.62 mmol), PdCl₂(PPh₃)₂ (214 mg, 305 μmol) and copper(I) iodide (58.0 mg, 305 μmol) in triethylamine (50 mL) and the reaction mixture was heated to reflux for 18 h. The solvent was then removed under reduced pressure and the residue was purified by flash column chromatography (silica gel; eluent, hexanes) followed by recrystallization from hot toluene to afford **S3** in 79% yield (1.66 g, 6.03 mmol) as a white solid.

$^1\text{H-NMR}$ (500.1 MHz CDCl_3): δ = 0.26 (s, 9 H, $\text{Si}(\text{CH}_3)_3$), 7.34–7.37 (m, 3 H, C_6H_5), 7.45 (m, 4 H, C_6H_4), 7.51–7.53 (m, 2 H, C_6H_5). $^{13}\text{C-NMR}$ (125.8 MHz, CDCl_3): δ = 0.06 ($\text{Si}(\text{CH}_3)_3$), 89.2, 91.4, 96.4, 104.8 ($\text{C}\equiv\text{C}$), 123.0, 123.1, 123.5, 128.5, 128.6, 131.5, 131.8, 132.0 (Ar). FT-IR (CH_2Cl_2) $\nu(\text{C}\equiv\text{C})$ 2156br. The product obtained via both methods gave identical analytical data, ^1H and ^{13}C NMR data were in agreement with those reported elsewhere.⁹

Preparation of 4-Ethynyltolan (S4).

A mixture of **S3** (1.11 g, 4.06 mmol), potassium carbonate (5.61 g, 40.6 mmol), methanol (50 mL), tetrahydrofuran (20 mL) and water (5 mL) was stirred at ambient temperature for 2 d and the solvents were removed under reduced pressure. Water (50 mL) was added to the residue, and the solids were isolated by filtration and washed with water (2×50 mL) to afford **S3** in 89% yield (727 mg, 3.60 mmol) as a white solid. $^1\text{H-NMR}$ (600.1 MHz CDCl_3): δ = 3.18 (s, 1 H, $\text{C}\equiv\text{C-H}$), 7.35–7.37 (m, 3 H, C_6H_5), 7.45 (m, 4 H, C_6H_4), 7.53–7.54 (m, 2 H, C_6H_5). $^{13}\text{C-NMR}$ (150.9 MHz, CDCl_3): δ = 79.0 ($\text{C}\equiv\text{C-H}$), 83.4, 89.0, 91.5 ($\text{C}\equiv\text{C}$), 122.0, 123.1, 123.9, 128.5, 128.7, 131.6, 131.8, 132.2 (Ar). ^1H and ^{13}C NMR data were in agreement with those reported elsewhere.¹⁰

Preparation of 4-Trimethylsilyl(ethynyl) bromobenzene (S5).

Ethynyltrimethylsilane (955 mg, 8.84 mmol) was added to a solution of 1-bromo-4-iodobenzene (2.50 g, 9.72 mmol), $\text{PdCl}_2(\text{PPh}_3)_2$ (62.0 mg, 88.4 μmol) and copper(I) iodide (17.0 mg, 88.4 μmol) in triethylamine (50 mL) and the reaction mixture was stirred at ambient temperature for 1.5 h. The solvent was then removed under reduced pressure and the residue was purified by flash column chromatography (silica gel; eluent, hexanes) to afford **S5** in 98% yield (2.20 g, 8.24 mmol) as a colourless oil which crystallised on standing to give a white crystalline solid. $^1\text{H-NMR}$ (400.1 MHz CDCl_3): δ = 0.12 (s, 9 H, $\text{Si}(\text{CH}_3)_3$), 7.18–7.20 (m, 2 H, C_6H_4), 7.29–7.31 (m, 2 H, C_6H_4). $^{13}\text{C-NMR}$ (100.6 MHz, CDCl_3): δ = 0.03 $\text{Si}(\text{CH}_3)_3$, 95.7, 104.0 ($\text{C}\equiv\text{C}$), 122.3, 122.9, 131.7, 131.9, 133.5 (Ar). FT-IR (CH_2Cl_2) $\nu(\text{C}\equiv\text{C})$ 2156 cm^{-1} . ^1H and ^{13}C NMR data were in agreement with those reported elsewhere.¹¹

Preparation of 4-Phenylethynyl-4'-(4-trimethylsilyl(ethynyl)phenylethynyl)benzene (**6**).^{12A} solution of **S4** (700 mg,

3.46 mmol), **S5** (876 mg, 3.46 mmol), Pd(PPh₃)₄ (160 mg, 138 μmol) and copper(I) iodide (26.0 mg, 138 μmol) in triethylamine was heated to reflux for 16 h, cooled to ambient temperature and the solvent was removed under reduced pressure. The residue remaining was Soxhlet extracted with toluene (120 mL) for 3 h, the solvent was removed and the residue recrystallized from toluene and ethanol to afford **6** as a tan solid in 49% yield (638 mg, 1.70 mmol). ¹H-NMR (600.1 MHz C₆D₆): δ = 0.25 (s, 9 H, Si(CH₃)₃), 6.05–7.02 (m, 3 H), 7.25 (m, 2 H), 7.30–7.35 (m, 6 H), 7.50–7.52 (m, 2 H). ¹³C-NMR (150.9 MHz, C₆D₆): δ = 0.0 (Si(CH₃)₃), 89.8, 91.5, 91.7, 92.1, 96.7, 105.5 (C≡C), 123.68, 123.71, 123.8, 123.9, 128.5, 128.7, 131.9, 131.95, 131.98, 132.0, 132.3 (Ar) one aromatic signal not observed, presumably obscured by the C₆HD₅ signal. ²⁹Si-NMR (119.2 MHz, C₆D₆): δ = -17.4.

2. Conductance Measurements: the *I(s)* technique and the BJ method.

All single molecule conductance measurements were recorded at room temperature in air with an Agilent 5500 SPM microscope. Molecular adlayers were formed on flame-annealed gold on glass samples from Arrandee, Schöer, Germany. These commercially available substrates were cleaned with acetone and flame-annealed with a butane torch until a slight orange glow was obtained. The gold slide was kept at this temperature for about 20 seconds during which time the butane torch was kept in motion around the sample to avoid overheating. This flame-annealing procedure was performed three times to generate flat Au (111) terraces over relatively large areas.¹³ Gold STM tips were fabricated from 0.25 mm Au wire (99.99%) which was freshly electrochemically etched for each experiment at +2.4 V in a mixture of ethanol (50%) and HCl (50%).

Electrical measurements were performed using an STM and both the *I(s)* method and the in situ break-junction (BJ). In the *I(s)* technique,¹⁴ a gold STM tip is brought to a fixed distance above the gold surface covered with an adlayer of the molecule under analysis. The initial approach distance of the STM tip to the substrate surface is determined by the characteristics of the STM and controlled by the set-point conditions, which are the bias voltage and set-point current (*I*₀). First the STM tip is located at a given height above the gold surface by setting the *I*₀ and *V*_{bias}. The feedback loop is then temporarily disabled and the tunneling current (*I*) is recorded as the STM tip is rapidly

retracted (s = distance). At the start of the retraction the target molecules can be trapped in the nanogap between the tip and surface and can become attached as a molecular bridge. As the tip is retracted the molecular bridge is then pulled up and stretched in the nano-junction until the molecular junction is broken. Under such circumstances, when the molecular bridge is formed there is typically a characteristic current plateau. As this junction is elongated to cleavage a step-like drop in the current is observed as the contact snaps. If during the tip retraction molecules are not caught in the STM nano-gap the current simply decreases exponentially with separation.

The in situ break-junction (BJ) method developed by Xu and Tao¹⁵ relies on the formation and cleavage of metallic break junctions between the STM tip and the metal substrate. Such metallic break junctions are formed by driving the STM tip a certain distance into the metal substrate. The STM tip is then retracted until the metal contact cleaves, which leaves a nano-gap into which molecular bridges can form. These molecular bridges then break upon further retraction of the STM tip and molecular conductance can be determined through statistical analysis of many such curves. The main difference between $I(s)$ and the in-situ BJ techniques is that the former method avoids direct metal-to-metal contact between the STM tip and substrate. However, a statistical analysis is generally used to generate histograms which are constructed from a large number of individual current (or conductance)-distance traces. Peaks occur in the conductance histograms when there are a significant numbers of common current plateaux in the collected current-distance curves and these peaks are attributed to single molecule conductance values for the target molecule.

3. Why is it necessary data selection for the TMSE anchor group?

Data selection is necessary for the TMSE anchor group due to the relatively low probability of forming molecular junctions (“hit rate” or junction formation probability¹⁶) when compared with other more conventional anchoring groups deployed in single molecule electronics. In the case of the in-situ break junction method, the “hit rate” can be considered as the probability of forming a molecular junction for one cycle in which the tip is driven into the surface and then retracted away to first cleave a Au-Au atomic point contact and then open a gap between the Au STM tip and substrate. A comparable definition is used for the $I(s)$ method. An estimate of the hit rate can be assessed by counting the number of retraction curves which show a recognizable current

plateau compared to the total number of retraction events undertaken. For compound **3**, which possesses TMSE anchors on both ends of the molecule, we find a hit rate of just 12 % with the in-situ BJ technique and a very similar value (9 %) with the $I(s)$ method. This hit rate is very low when compared with other anchoring groups, where hit rates of up to 100 % have been reported.¹⁷ An example of the latter is the dihydrobenzo[*b*]thiophene linker (and oligoene molecular bridges¹⁷). With high hit rate anchor groups, for instance pyridyl, we are able to routinely construct histograms without data selection. However, for the low hit rate TMSE anchor groups it is necessary to select the curves that show junction formation events, recognized by their plateau and step structure, from the majority of retraction traces in which no junction forms. For this reason we have to use trace selection for the TMSE contacts to resolve a clear peak in the conductance histogram (Figure S1). The low hit rate for TMSE contacts is also consistent with the anchoring configuration discussed in the main text and garnered from DFT modeling.

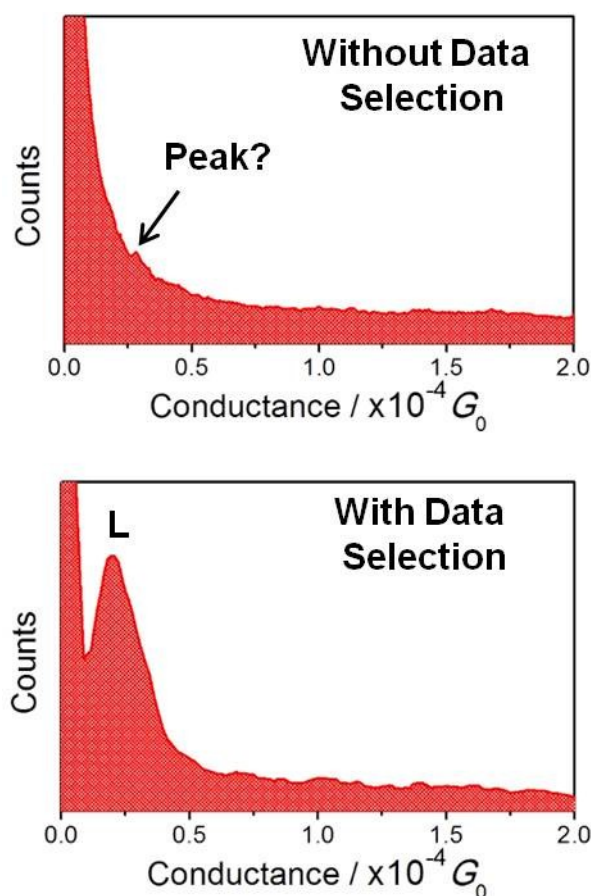


Figure S1. Conductance histograms built from summation of all recorded conductance traces by using the $I(s)$ method for compound **3**, without data selection (top) and with

data selection (bottom): from all conductance traces (ca. 450) that showed discernible plateaus (with a current plateau which exceeds 0.1 nA in length) such as those displayed in the inset of the Figure 2c right.

4. Determination of the L-conductance peak by using the BJ technique for compounds 1 and 2.

A more detailed analysis closer to, but just above, the noise level of the current amplifier in the BJ scans shows another set of pronounced peaks located at ca. $2.5 \times 10^{-5} G_0$ for **1** (Figure S1a) and at ca. $2.5 \times 10^{-5} G_0$ for **2** (Figure S2b) which are in good agreement with the L-conductance peak obtained by using the $I(s)$ method for both compounds, see Figure 3 and Table 1 in main text.

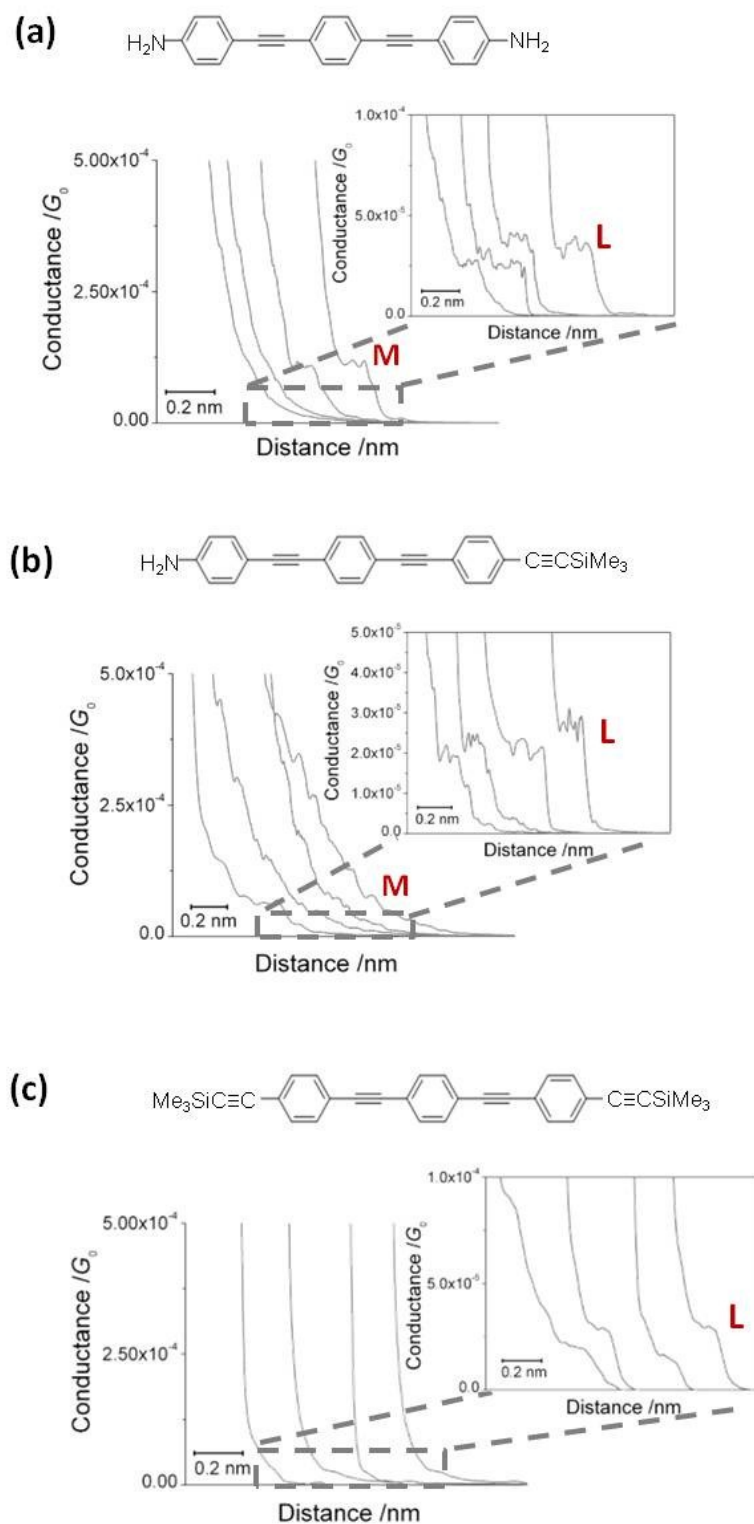


Figure S2. Conductance traces recorded by using the BJ method for (a) **1**, (b) **2** and (c) **3**. The insets show a more detailed analysis closer to the noise level of the current amplifier where another set of pronounced plateaux is observed and in good agreement with the L-conductance peak obtained by using the $I(s)$ method for all compounds (see Figure 2 and Table 1).

5. Study of TMS-capped ligand in gold nanoparticles (AuNPs) phase-transfer.

To further study the stability of the terminal TMS moiety in the presence of Au, TMS-capped gold nanoparticles (AuNPs) were synthesized. Alkyne-capped nanoparticles have been studied several times in the past, and simple phase-transfer ligand exchange¹⁸ (water-organic solvent) gave excellent results. Therefore, we reasoned that the TMS group, as a weaker ligand, should allow little or no transfer of AuNPs to the organic phase, and if we observed phase transfer, we could further investigate the TMS-capped AuNPs by Raman Spectroscopy.

We synthesised the nanoparticles as ligand free water dispersion using the method developed by Martin et al.¹⁹ The solution was then diluted with acetone (as phase transfer agent) and capping ligands in 1 mM concentration were prepared as benzene and hexane solutions. Figure S3 shows the structure of the compounds used.

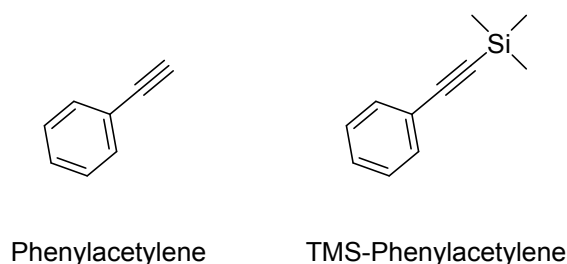


Figure S3: Structures of capping ligand used in this study.

TMS-capped ligand do not perform well as AuNPs phase transfer ligands. The TMS moiety does not cleave in the presence of Au, as can be seen from the different behaviour in TMS-phenylacetylene and unprotected phenylacetylene Figure S4 and S5. In benzene, TMS-capped nanoparticles are transferred quantitatively to the organic layer, but the ligand is too weak to prevent aggregation and precipitation. In hexane, possibly due to the non-polar nature of the solvent, TMS-capped ligands fail to transfer completely the nanoparticles, and the small amount that is slowly transferred suffers from aggregation and precipitation. On the contrary, unprotected phenylacetylene performed much better as capping ligand, promoting complete phase transfer in both solvents. A small degree of aggregation is observed, and this is in good agreement with the published literature.¹⁹

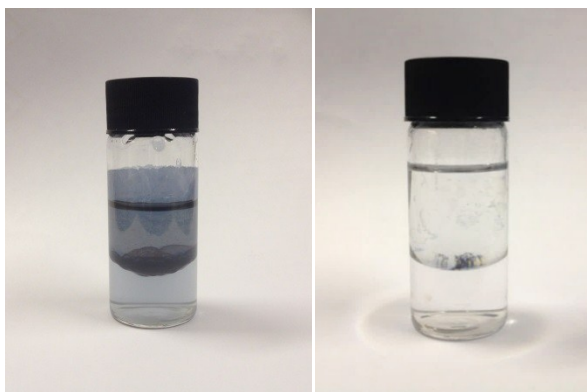


Figure S4. Water: Benzene phase transfer. Slight aggregation of the NPs (trapped at the liquid-liquid interface and on the wall surface of the glass vial) is evident when phenylacetylene was used as a capping ligand (left) and complete precipitation of the NPs occurred when TMS-Phenylacetylene was used (right).

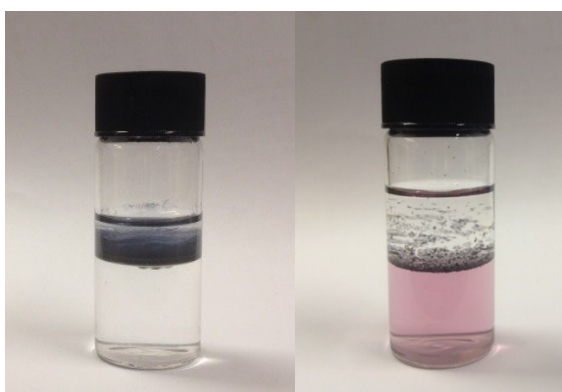


Figure S5. Water: Hexane phase transfer. Slight aggregation of the NPs (as inferred from the change in colour) and complete transfer when phenylacetylene was used as a capping ligand (left), but only partial transfer of AuNPs and precipitation when TMS-Phenylacetylene was used (right).

6.- QCM measurements.

Quartz Crystal Microbalance (QCM) measurements were carried out using a Stanford Research System instrument, with a frequency counter with 0.1 Hz resolution, and employing AT-cut, α -quartz crystals with a resonant frequency of 5 MHz having circular gold electrodes patterned on both sides. A QCM resonator was incubated in a 0.01 mM solution of **3**, **4** and **5** in chloroform for 24 h.

Afterwards the substrate was thoroughly rinsed with chloroform and dried. The variation of the resonant frequency of the substrates before and after incubation was determined. This value is directly related with the mass incorporated on the QCM substrate by means of the Sauerbrey equation which establishes that:²⁰

$$\Delta f = -\frac{2 \cdot f_0^2 \cdot \Delta m}{A \cdot \rho_q^{1/2} \cdot \mu_q^{1/2}} \quad (1)$$

where f_0 is the fundamental resonant frequency of 5 MHz, Δm (g) is the mass change, A is the electrode area, ρ_q is the density of the quartz ($2.65 \text{ g}\cdot\text{cm}^{-3}$), and μ_q is the shear module ($2.95 \cdot 10^{11} \text{ dyn}\cdot\text{cm}^{-2}$).

7. Analysis of the length of the plateaus of all I (s) scans for the L-group for compounds **1 and **3**.**

Long current plateaus can indicate a flexible array of available surface-molecule binding configurations within the junction. A good example of such behavior involves amine terminal groups and gold contacts, with the amine group able to accommodate different attachment points and geometrical aspects such as a broader range of Au-N-C bond angles and giving relatively long plateaux.²¹ The average lengths of the current plateaux for the L-conductance group of **1** (amine termini), **2** (amine and TMSE termini) and **3** (TMSE termini) are compared in Figure S6 (this analysis is obtained for the same data as in Figure 2). The average length of the plateaux for **1** is longer than for **2** and **3**, 0.23 ± 0.10 , 0.19 ± 0.07 and 0.17 ± 0.09 nm, respectively. The shorter plateaux for the TMSE anchor groups are consistent with a specific and rather unaccommodating contact geometry of the TMSE contacts, which are unable to adapt to changes in the molecule-electrode separation without rupture of the metal|molecule|metal junction.

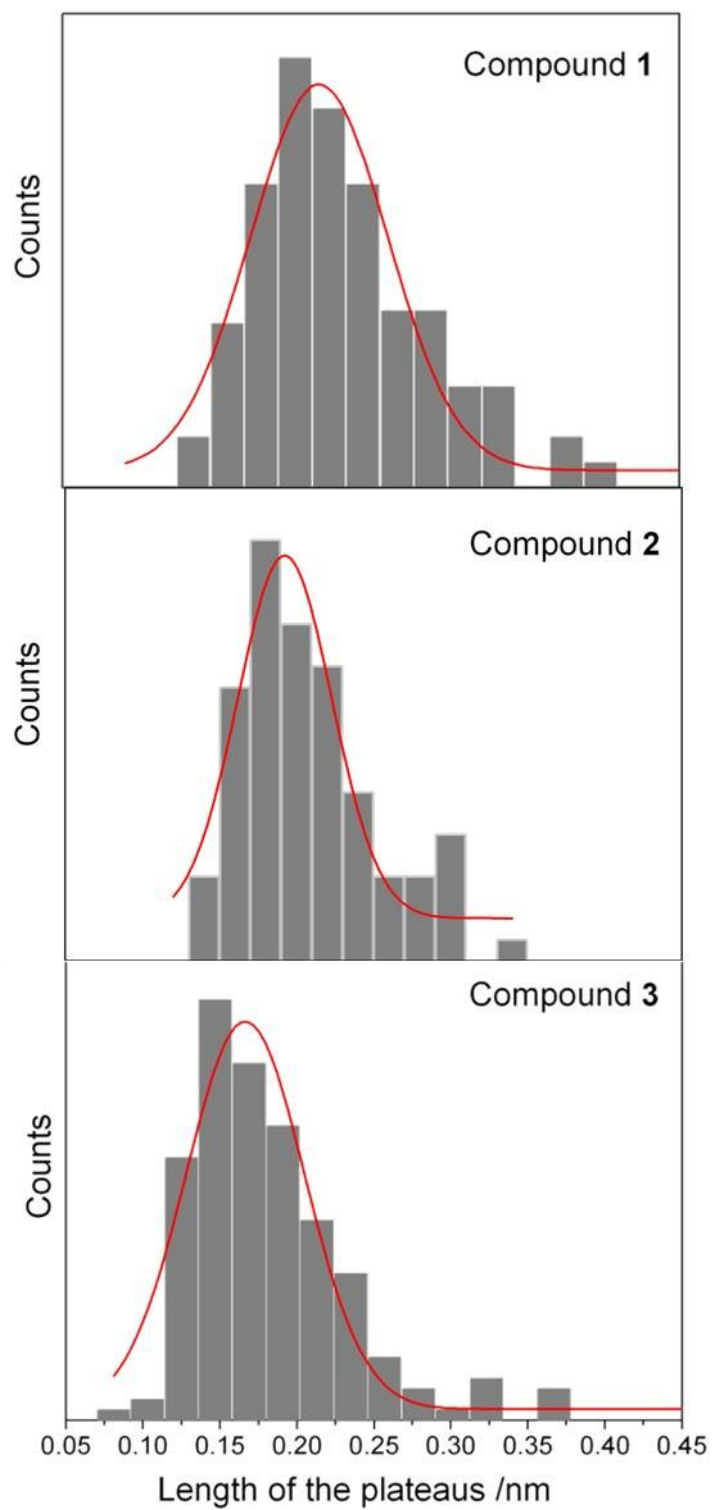


Figure S6. Histograms of the length of the plateaus for all $I(s)$ scans used to build the histograms showed in Figure 2 for the L-group of **1** (top), **2** (middle) and **3** (bottom).

8. Theoretical methods.

Ab-initio parameters

We used a double- ζ polarized basis set (DZP) for all elements in the molecule and a single- ζ polarized (SZP) basis set which explicitly included the d states²² and diffuse orbitals for the gold atoms at the electrodes. The choice of a simpler basis set for gold dramatically decreases the execution time of the simulations and gives results similar to those obtained with more involved basis sets.²³ We indeed checked that the transmission of the studied molecules calculated with SZP + diffuse orbitals on the electrodes was qualitatively similar and gave the same transmission at the Fermi level as that obtained with DZP on the electrodes. We found however that, in order to accurately determine the charge transfer between the electrodes and the molecule we had to include the DZP basis on the electrodes. DZP was therefore necessary to correctly describe the bonding nature between the molecule and the electrodes. We also used ghost states to remove the basis set superposition error (BSSE) in the calculation of the binding energies. We represented the density, the potential, the Hamiltonian and the overlap matrix elements in a real space grid defined with an energy cutoff of 200 Ry. We used the local density approximation (LDA) for the exchange and correlation energy and potential as parametrized by Perdew and Zunger.²⁴ We relaxed the molecular coordinates in the gas phase using a conjugated gradient method until all forces were smaller than 0.05 eV/Å.

The relaxed coordinates were then placed between the surfaces. We performed molecular dynamics (MD) on each configuration with a fixed distance d between the two surfaces. We used a Nose thermostat, with initial and target temperatures set to $T = 300$ K and we allowed, for each configuration, 300 molecular dynamics steps, with a time step length of 1 fs. For configuration 3, we employed 400-600 time steps to build better statistics. The conductance was calculated every 10 steps, and the resulting values organized to construct a theoretical conductance histogram for comparison with the experimental data. As a consequence, each histogram contains about 120-150 conductance values.

Transport calculations

Gollum²⁵ is a new-generation transport code that calculates the electronic contribution to charge, spin and thermal transport of a solid-state junction comprised of

an arbitrary number of leads and a scattering region. To do so, it reads the Hamiltonians of each lead and of the scattering region from a DFT program like SIESTA. In the present article, we have used leads made of bulk gold electrodes grown along the (111) crystallographic direction. We have picked as Principal Layer in the leads a cell containing three atomic layers of 6 x 6 atoms each. We have chosen for the scattering region a cell containing the central part of the junction: the surface region of the electrodes and attached to them, one of the molecules under consideration here. We have chosen for the surface of each gold (111) electrode five atomic layers consisting of 6 x 6 atoms each. By doing so, we ensure a smooth matching of the leads and the scattering region Hamiltonians and, at the same time we provide enough buffer space to achieve an adequate electronic screening of the disturbance provided by the presence of the surfaces and the molecule. We have used the Γ point (1 k point) along the plane perpendicular to the transport direction, which in the case of gold is enough to achieve convergence.

This method improves the bare DFT conductance results^{23,26,27} and usually leads to almost quantitative agreements between experiments and theory. We have performed detailed analyses to optimize the junction geometries and reproduce the experimental conditions.

Corrections to the transport properties

To correct for the deficient molecular HOMO and LUMO energy positioning and their gap predicted by DFT, we have included the phenomenological spectral adjustment known as SAINT (spectral adjustment in nanoscale transport).^{22,28-30} SAINT repositions the HOMO and LUMO energy levels to their correct position. To do that, we first calculate the ionization potential (IP) and electron affinity (EA) of each molecule in the gas phase. We also take into account that the presence of a metallic surface at a distance a from the molecule screens the IP and EA. An approximate formula that picks this effect is given by $W = -e2\ln 2/(8\pi\epsilon_0a) = 4.99/a$ eV; $a = d/2 - 1$ Å, where d is the distance between surfaces. We note that variations of up to 1 Å in this distance do not affect significantly the resulting values of the conductance. The values of the HOMO, LUMO, IP, EF and the gas phase corrections are given in Table 1. The distance between the center of the molecule and the charge plane, the image charge

corrections and the final corrections for some ideal coupling configurations are given in Table 2.

Table 1. Energy of the HOMO, LUMO, ionization potential (IP) and electron affinity (EA), size of the DFT and ΔE_{SCF} gaps, and gas phase corrections for the HOMO and LUMO (all in eV).

Compound	HOMO	LUMO	DFT gap	IP	EA	ΔE_{SCF} gap	$\Sigma_{\text{GP,H}}$	$\Sigma_{\text{GP,L}}$
1	-4.47	-2.30	2.17	6.10	0.62	5.48	-1.63	1.68
2	-4.80	-2.84	1.96	6.43	1.26	5.17	-1.63	1.58
3	-5.25	-3.18	2.07	6.70	1.73	4.97	-1.45	1.45

Table 2. Distance between the molecular charge and the image plane (a , in Å), image charge correction (W , in eV) and final corrections (in eV) for all compounds.

Compound 1	a	W	Σ_{H}	Σ_{L}
Adatom-Adatom	13.96	0.36	-1.27	1.32
Adatom-Bridge	12.48	0.40	-1.23	1.28
Bridge-Bridge	10.99	0.45	-1.18	1.23

Compound 2	a	W	Σ_{H}	Σ_{L}
Adatom-Adatom	15.36	0.32	-1.31	1.26
Adatom-Top	14.49	0.34	-1.29	1.24
Bridge-Adatom	13.88	0.36	-1.27	1.22
Bridge-Top	13.00	0.38	-1.25	1.20

Compound 3	a	W	Σ_{H}	Σ_{L}
Adatom-Adatom	16.77	0.30	-1.15	1.15
Adatom-Top	15.89	0.31	-1.14	1.14
Top-Top	15.02	0.33	-1.12	1.12

9.- Influence of the bin size selection in the theoretical conductance histogram .

Figure S4 shows two different bin sizes selected for building the theoretical conductance histogram derived from the MD simulations for compound 1. As it can be observed, this results in slightly different grouping and width of the conductance peaks

so, the larger the bin size, the larger the number of results that are assigned to a certain conductance.

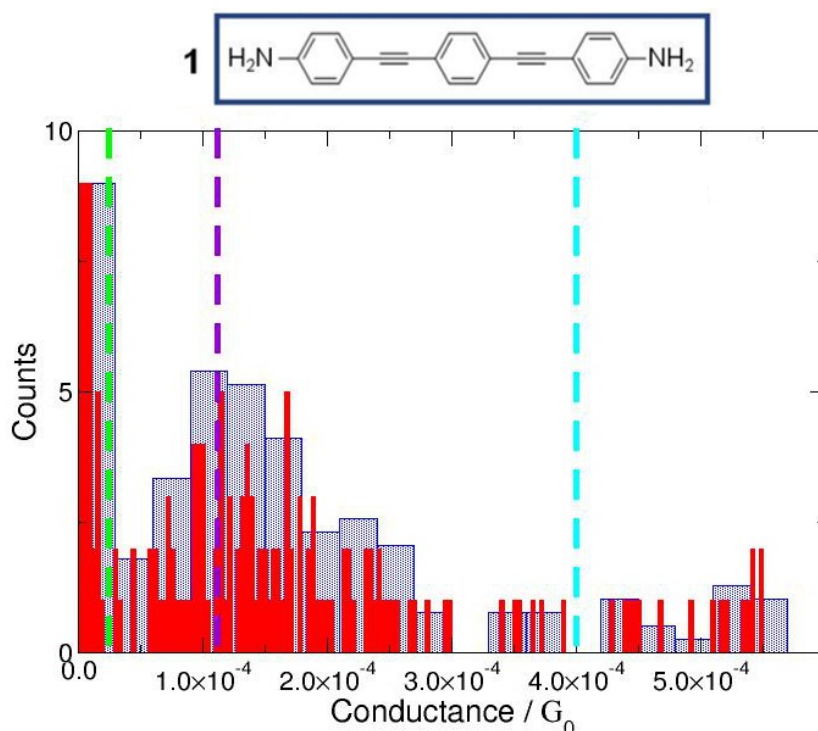


Figure S7. Conductance histogram of **1** as a function of the bin size selected.

References

- (1) Mihigo, S. O.; Mammo, W.; Bezabih, M.; Andrae-Marobela, K.; Abegaz, B. M. *Bioorgan Med Chem* **2010**, *18*, 2464.
- (2) Miyaura, N.; Suzuki, A. *Org Synth* **1990**, *68*, 130.
- (3) Cross, T. A.; Davis, M. C. *Synthetic Commun* **2008**, *38*, 499.
- (4) Kubel, C.; Chen, S. L.; Mullen, K. *Macromolecules* **1998**, *31*, 6014.
- (5) Demessence, A.; Long, J. R. *Chem-Eur J* **2010**, *16*, 5902.
- (6) Fulmer, G. R.; Miller, A. J. M.; Sherden, N. H.; Gottlieb, H. E.; Nudelman, A.; Stoltz, B. M.; Bercaw, J. E.; Goldberg, K. I. *Organometallics* **2010**, *29*, 2176.
- (7) Turp, D.; Wagner, M.; Enkelmann, V.; Mullen, K. *Angew Chem Int Edit* **2011**, *50*, 4962.
- (8) Nierengarten, J. F.; Zhang, S.; Gegout, A.; Urbani, M.; Armaroli, N.; Marconi, G.; Rio, Y. *J Org Chem* **2005**, *70*, 7550.
- (9) Lydon, D. P.; Porres, L.; Beeby, A.; Marder, T. B.; Low, P. J. *New J Chem* **2005**, *29*, 972.
- (10) Stalder, R.; Xie, D. P.; Zhou, R. J.; Xue, J. G.; Reynolds, J. R.; Schanze, K. S. *Chem Mater* **2012**, *24*, 3143.
- (11) Rahaim, R. J.; Shaw, J. T. *J Org Chem* **2008**, *73*, 2912.

- (12) Hwang, J. J.; Tour, J. M. *Tetrahedron* **2002**, *58*, 10387.
- (13) Haiss, W.; Lackey, D.; Sass, J. K.; Besocke, K. H. *J Chem Phys* **1991**, *95*, 2193.
- (14) Haiss, W.; van Zalinge, H.; Higgins, S. J.; Bethell, D.; Hobenreich, H.; Schiffrin, D. J.; Nichols, R. J. *J Am Chem Soc* **2003**, *125*, 15294.
- (15) Xu, B. Q.; Tao, N. J. *Science* **2003**, *301*, 1221.
- (16) Manrique, D. Z.; Huang, C.; Baghernejad, M.; Zhao, Z.; Al-Owaedi, O. A.; Sadeghi, H.; Kaliginedi, V.; Hong, W.; Gulcur, M.; Wandlowski, T.; Bryce, M. R.; Lambert, C. J. *Nature Communications* **2015**, *6*, 6389.
- (17) Moreno-Garcia, P.; Gulcur, M.; Manrique, D. Z.; Pope, T.; Hong, W. J.; Kaliginedi, V.; Huang, C. C.; Batsanov, A. S.; Bryce, M. R.; Lambert, C.; Wandlowski, T. *J Am Chem Soc* **2013**, *135*, 12228.
- (18) Maity, P.; Takano, S.; Yamazoe, S.; Wakabayashi, T.; Tsukuda, T. *J Am Chem Soc* **2013**, *135*, 9450.
- (19) Martin, M. N.; Basham, J. I.; Chando, P.; Eah, S. K. *Langmuir* **2010**, *26*, 7410.
- (20) Sauerbrey, G. *Z Phys* **1959**, *155*, 206.
- (21) Kamenetska, M.; Quek, S. Y.; Whalley, A. C.; Steigerwald, M. L.; Choi, H. J.; Louie, S. G.; Nuckolls, C.; Hybertsen, M. S.; Neaton, J. B.; Venkataraman, L. *J Am Chem Soc* **2010**, *132*, 6817.
- (22) Garcia-Suarez, V. M.; Lambert, C. J. *New J Phys* **2011**, *13*, 053026
- (23) Kaliginedi, V.; Moreno-Garcia, P.; Valkenier, H.; Hong, W. J.; Garcia-Suarez, V. M.; Buitter, P.; Otten, J. L. H.; Hummelen, J. C.; Lambert, C. J.; Wandlowski, T. *J Am Chem Soc* **2012**, *134*, 5262.
- (24) Perdew, J. P.; Zunger, A. *Phys Rev B* **1981**, *23*, 5048.
- (25) Ferrer, J.; Lambert, C. J.; Garcia-Suarez, V. M.; Manrique, D. Z.; Visontai, D.; Oroszlany, L.; Rodriguez-Ferradas, R.; Grace, I.; Bailey, S. W. D.; Gillemot, K.; Sadeghi, H.; Algharagholy, L. A. *New J Phys* **2014**, *16*, 093029.
- (26) Wang, C. S.; Batsanov, A. S.; Bryce, M. R.; Martin, S.; Nichols, R. J.; Higgins, S. J.; Garcia-Suarez, V. M.; Lambert, C. J. *J Am Chem Soc* **2009**, *131*, 15647.
- (27) Sedghi, G.; Garcia-Suarez, V. M.; Esdaile, L. J.; Anderson, H. L.; Lambert, C. J.; Martin, S.; Bethell, D.; Higgins, S. J.; Elliott, M.; Bennett, N.; Macdonald, J. E.; Nichols, R. J. *Nat Nanotechnol* **2011**, *6*, 517.
- (28) Neaton, J. B.; Hybertsen, M. S.; Louie, S. G. *Phys Rev Lett* **2006**, *97*, 216405.
- (29) Quek, S. Y.; Venkataraman, L.; Choi, H. J.; Louie, S. G.; Hybertsen, M. S.; Neaton, J. B. *Nano Lett* **2007**, *7*, 3477.
- (30) Kristensen, I. S.; Mowbray, D. J.; Thygesen, K. S.; Jacobsen, K. W. *J Phys-Condens Mat* **2008**, *20*, 374101.